Astron. Astrophys. 352, 217–227 (1999)

ASTRONOMY AND ASTROPHYSICS

Evolution of X-ray activity and rotation on G-K giants

P. Gondoin

Astrophysics Division, European Space Agency – Postbus 299, 2200 AG Noordwijk, The Netherlands (pgondoin@astro.estec.esa.nl)

Received 20 July 1999 / Accepted 20 September 1999

Abstract. The recent availability of stellar parallaxes provided by the Hipparcos star catalogue (ESA 1997) enables an accurate determination of the positions of single field giants in a theoretical H-R diagram and a reliable estimate of their masses. The present study combines these new astrometric data with previously published X-ray fluxes and rotational velocities. The results confirm the existence of a sharp decrease of X-ray emission at spectral type K1 for 2.5 $M_\odot < M < 5\ M_\odot$ giants. The study shows that the rotational velocity of these stars reaches a minimum at the same location in the H-R diagram. However, no tight relationship between X-ray luminosities and projected equatorial velocities was found among the sample stars. I suggest that these results could reflect the importance of differential rotation in determining the level of coronal emission among $\geq$ 2.5 $M_\odot$ G and K giants. The restoration of rigid rotation at the bottom of the red giant branch could prevent the maintenance of large scale magnetic fields, thus explaining the sharp decrease of coronal X-ray emission at spectral type K1.

Key words: stars: activity – stars: evolution – stars: late-type

1. Introduction

One major topic of stellar activity is to explain how phenomena seen on the Sun and stars, and especially magnetic phenomena, depend on stellar parameters such as rotation rate, mass, and age. One magnetic field diagnostic for cool stars is coronal X-ray emission. The yellow and red giants form an appropriate class of stars for studying effects resulting from the variation of these stellar parameters (Gondoin et al. 1987). In particular, 2.5 $M_\odot < M < 5\ M_\odot$ giants have A and late B type progenitors on the main sequence which have no outer convection zones and which are typically rapid rotators. As they evolve off the main sequence, in the shell hydrogen burning stage, they develop thin outer convection zones. These giants then rapidly traverse the F and G spectral types zone of the H-R diagram which is relatively devoid of stars and is known as "the Hertzsprung gap". During this rapid evolution, the internal structure of these stars changes substantially. The thin convective shells prior to early G give way to rapidly deepening convection zones at mid-late G. The increasing convection zone depth combined with fast rotation is likely to trigger dynamo processes which generate the magnetic fields that, by analogy with the Sun, cause the X-ray emission of the outer stellar atmospheres. A large fraction of the yellow giants are able to hold their high rotation till mid-G spectral types. At this point, rotation velocities measurements (Gray 1989) indicate a strong rotational braking during their further evolution across the Hertzsprung gap. Also, a transition among late type giants from hot coronae and transition regions to cool winds is indicated by various dividing lines in the H-R diagram. These include the X-ray dividing line (XDL) which lies in the H-R diagram around spectral type K1 (Ayres et al. 1981). Hence, the yellow and red giants form a natural laboratory to measure the effect of rotation on the generation of stellar magnetic fields. However, no conclusive connection has been established between the X-ray coronal emission of giants and the evolution of their rotation rates partly because X-ray fluxes and rotational velocities have been measured on different samples of stars with imprecisely known masses and evolutionary status.

The recent availability of stellar parallaxes provided by the Hipparcos star catalogue (ESA 1997) enables an accurate determination of the positions of single field giants in a theoretical H-R diagram and a reliable estimate of their masses. The present study combines these new astrometric data with previously published X-ray fluxes, rotational velocities and lithium abundances. It provides a revised insight on the connection between activity and rotation during the evolution of cool giants. Sect. 2 of this paper describes the selection of the sample giants. Their evolutionary status is inferred in Sect. 3 from comparison with stellar models and lithium abundance measurements. Sect. 4 presents a data survey of rotational velocities and X-ray luminosities measurements. The evolution of solar-type activity along the red giant branch and possible relationships with the evolution of stellar rotation are discussed in Sect. 5.

2. Sample selection

A first list of candidate single G-K giants was established using the samples of Haisch et al. (1990) and Maggio et al. (1990). These authors have selected all the optical candidates in the Bright Star Catalogue and its supplement (Hoffleit et al. 1984) with spectral types in the range F to M. Of the optically selected

HD	Spectral type	V	par (mas)	$T_{\rm eff}$ (K)	[Fe/H]
3546	G8 III	4.34	19.34	4640	-0.69
4128	K0 III	2.04	34.04	4840	0.03
4188	K0 III	4.77	15.54	4770	0.02
5395	G8 IIIb	4.62	15.84	4790	-0.67
6805	K1.5 III	3.46	27.73	4520	0.01
6833	G9 III	6.75	4.35	4410	-0.97
8763	K1 III	5.50	10.63	4560	-0.12
9927	K3 III	3.59	18.76	4440	-0.01
10380	K3 IIIb	4.45	8.86	4050	-0.29
12929	K2 III	2.01	49.48	4520	-0.21
17709	K5 III	4.56	7.97	3880	-0.36
18322	K1 III	3.89	24.49	4670	0.10
25604	K0 III	4.36	18.04	4700	0.01
28100	G7 IIIa	4.69	7.17	4830	-0.28
28292	K2 III	4.96	16.78	4520	-0.17
28305	G9.5 III	3.53	21.04	4810	0.00
28307	K0 IIIb	3.84	20.66	4960	0.04
32887	K4 III	3.19	14.39	4000	-0.17
40409	K1 III-IV	4.65	36.67	4760	0.10
43039	G8.5 IIIb	4.32	19.31	4580	-0.27
47205	K1 III+	3.95	50.41	4800	0.04
59294	K1 III	4.55	5.82	4370	0.02
73108	K1 III	4.59	12.92	4390	-0.23
74772	G5 III	4.05	14.27	5210	-0.03
76294	G9 II-III	3.11	21.64	4770	0.04
82210	G4 III-IV	4.54	30.89	5280	-0.36
85444	G6/G8 III	4.11	11.92	5000	-0.14
89485	G7 IIICN	2.01	25.96	4690	-0.43
93813	K0/K1 III	3.11	23.54	4330	-0.30
95272	K1 III	4.08	18.71	4490	-0.06
98839	G7.5 IIIa	4.99	6.63	4880	0.09
102328	K3 III	5.27	15.80	4250	0.09
105707	K2 III	3.02	10.75	4320	-0.13
113226	G8 III	2.85	31.90	4960	0.03
117876	G8 III	6.11	6.94	4580	-0.50
124897	K1.5 III	-0.05	88.85	4290	-0.46
129989	K0 II-III	2.35	15.55	4780	0.18
131873	K4 III	2.07	25.79	4190	-0.26
133208	G8 IIIa	3.49	14.91	4920	0.33
136726	K4 III	5.02	8.37	4120	0.07
140573	K2 IIIb	2.63	44.54	4490	0.16
141714	G3.5 III	4.59	19.71	5240	-0.16
143107	K2 III	4.14	14.20	4320	-0.32
145001	G8 III	5.00	8.40	4990	-0.26
148387	G8 IIIb	2.73	37.18	4990	-0.13
151680	K2.5 III	2.29	49.85	4530	-0.23
153210	K2 III	3.19	37.99	4580	0.00
159966	K0 III	5.07	15.02	4680	-0.20
163917	G9 III	3.32	21.35	4880	0.10
163993	G8 III	3.70	24.12	5010	0.12
192806	K3 III	4.50	9.94	4170	-0.03
205435	G8 III	3.98	26.20	5210	-0.17
216131	G8 III	3.51	27.95	5010	-0.09
222404	K1 IV	3.21	72.50	4840	-0.04

HD	V	$B-V$	$V-I$	par (mas)	$T_{\rm eff}$ (K)
6903	5.57	0.697	0.75	8.09	5270
7578	6.04	1.163	1.12	10.36	4560
13137	6.31	0.948	0.94	5.53	4900
13222	6.25	0.915	0.91	7.44	4950
18884	2.54	1.630	1.97	24.49	3470
19637	6.02	1.278	1.17	8.03	4420
19735	6.32	1.425	1.38	6.50	4120
19845	5.93	0.972	0.96	10.47	4860
61338	5.04	1.616	1.72	6.13	3680
69994	5.80	1.137	1.10	6.39	4600
71243	4.05	0.413	0.49	51.40	5730
82668	3.16	1.538	1.59	13.72	3860
83805	5.61	0.951	0.94	9.59	4890
92095	5.55	1.270	1.23	6.34	4380
96566	4.62	0.988	0.97	8.82	4840
100029	3.82	1.613	1.79	9.76	3630
100055	6.54	0.937	0.93	6.94	4910
109742	5.70	1.436	1.43	6.29	4070
111812	4.93	0.681	0.70	10.62	5320
113994	6.15	0.997	0.98	8.64	4820
119081	6.22	1.311	1.27	8.54	4310
121107	4.77	0.845	0.86	4.77	5050
138852	5.74	0.976	0.96	10.24	4860
140117	6.45	1.102	1.06	7.36	4660
140815	6.32	1.195	1.15	5.27	4510
145000	6.25	1.140	1.10	6.92	4600
146084	6.30	1.148	1.11	9.75	4580
148374	5.67	0.956	0.94	7.91	4890
151101	4.84	1.212	1.19	4.79	4460
154391	6.16	1.006	0.98	9.24	4810
160538	6.61	1.043	1.01	9.68	4760
211833	5.75	1.256	1.21	4.73	4410
214952	2.07	1.610		19.17	3750
220657	4.42	0.617	0.67	18.83	5400

HD	V	$B-V$	$V-I$	par (mas)	$T_{\rm eff}$ (K)
FK Com	8.15	0.870	0.93	4.27	4970
YY Men	8.06	1.076	1.04	3.43	4700
33798	6.91	0.982	0.96	8.94	4850
199178	7.23	0.785	0.82	10.68	5140
223460	5.86	0.806	0.83	7.41	5110

Table 1. Stellar parameters and parallaxes of the sample giants. The left table lists single giants with spectrally derived effective temperatures extracted from the catalogue of [Fe/H] determination from Cayrel de Strobel (1996). [Fe/H] is the logarithmic difference between the relative abundance of iron in the atmosphere of a giant and in the solar atmosphere. The upper right table lists single giants for which effective temperatures have been derived from Hipparcos $B-V$ and $V-I$ color indices. Candidate FK Comae stars with photometrically derived temperatures are listed in the lower right table.

HD	$M/M_\odot$	$v \sin i$ (km s^{-1})	L_X (10^{27} erg s^{-1})	log(ϵ(Li))
3546		4.2	< 13	< 0.5
4128	3.2	4.0	368–1138	< 0.2
4188				< 0.3
5395				< 0.2
6805			4	1.1
6833	2.1			
8763		2.1	< 80	
9927	2.3			
10380	1.9			
12929	2.0	1.0	< 4	< 0.0
17709	2.0			< -1.5
18322				
25604		1.0	< 80	< 0.0
28100	4.0	3.9	< 251	
28292		1.0		
28305	2.7		11–21	1.2
28307		1.5	1996	
32887	2.1			-0.2
40409	1.2		9	
43039				< 0.2
47205	1.3			< 0.0
59294	4.0			0.5
73108	1.9	1.0	< 126	
74772	3.2	5.8	< 126	
76294	2.9	2.1	< 16	< 0.5
82210	1.9	5.5	307–901	
85444	3.5	2.9	2408	
89485	3.8	1.2	< 26	
93813	2.0		66	< -0.4
95272	1.8			< 0.0
98839	3.8		107	0.7
102328	1.0	1.0	72	< -0.4
105707	4.4			0.8
113226		2.3	20–86	
117876	2.1	2.8		
124897	2.1	1.0	< 4	< -0.8
129989	4.6	8.4	< 51	
131873	2.8	1.6	< 10	
133208	3.6		107–153	1.2
136726	1.7	1.6	< 64	
140573		1.5	< 5	< 0.0
141714	2.4		1456	
143107	2.0	1.0	< 51	< -0.3
145001	3.4	9.4	3318	< 0.5
148387		1.2	6	
151680			1.5	
153210		1.0	< 13	< 0.0
159966		1.0	< 64	
163917	3.0			
163993			357–920	1.3
192806	1.9			0.5
205435	2.4		114–343	0.9
216131		1.2	1.1	< 0.5
222404	1.4		1.4	< 0.0

HD	$M/M_\odot$	$v \sin i$ (km s^{-1})	L_X (10^{27} erg s^{-1})	log(ϵ(Li))
6903	2.8	70	692	
7578		1.6		
13137	3.0	1.1		
13222		1.3	388	
18884	1.3			
19637	2.2	1.8		
19735	1.2	2.1		
19845		1.6		< 0.3
61338	1.7	2.0		
69994	2.7	1.5		
71243	1.0	28.3	84	
82668	2.0			
83805		1.2	< 50	
92095	2.5	1.5		
96566	3.6			
100029	1.7			
100055		2.5		
109742	1.6	2.0		
111812	2.8	63	6325	
113994		1.8		
119081	1.3	1.3		
121107	4.5	14.5	3718	< 1.2
138852		1.0		< 0.3
140117		1.3		
140815	2.5	1.0		
145000	2.2	1.6	3659	< 0.0
146084		1.9		
148374	2.9	3.3	248	0.4
151101	3.5			
154391		1.0		
160538	1.8			
211833	3.1	2.0		
214952	2.4			
220657	2.3	33.7	1381	

HD	$M/M_\odot$	$v \sin i$ (km s^{-1})	L_X (10^{27} erg s^{-1})	log(ϵ(Li))
FK Com	2.2	162.5	74.54-9415.6	
YY Men	2.2	45	26215	1.6–2.0
33798	1.8	29	1074.7	1.8
199178	1.7	80	10402	
223460	2.9		8203.7	

Table 2. Mass estimates, rotational velocities (Medeiros & Mayor 1995, Gray 1989), X-ray luminosities (Maggio et al. 1990, Hünsch et al. 1998) and lithium abundances (Brown et al. 1989) of the spectroscopic subsample (left), the photometric subsample (upper right) and the FK Comae candidates (lower right). Stellar masses have been estimated from Schaller et al. (1992) evolutionary tracks assuming a first crossing of the H-R diagram. Masses of stars located in the red giant clump region are not provided due to the uncertainty on their evolutionary status.

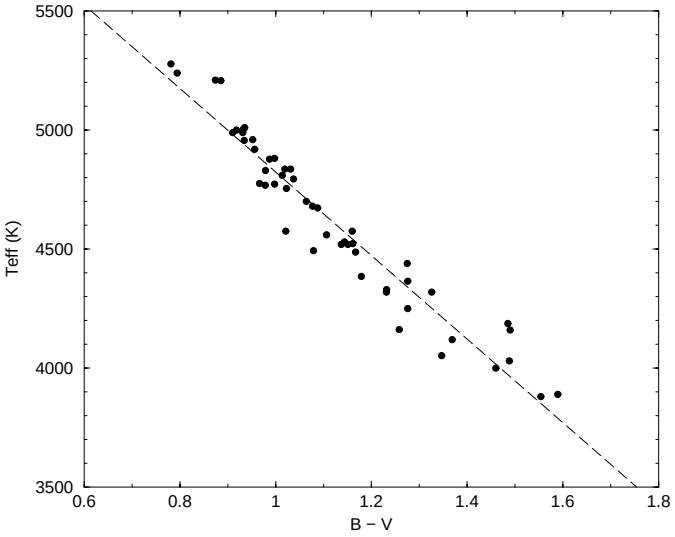

Fig. 1. Spectrally determined effective temperatures of sample giants versus $B-V$ color indices extracted from the Hipparcos catalogue. The dashed curve represents the calibration curve described by Eq. (1).

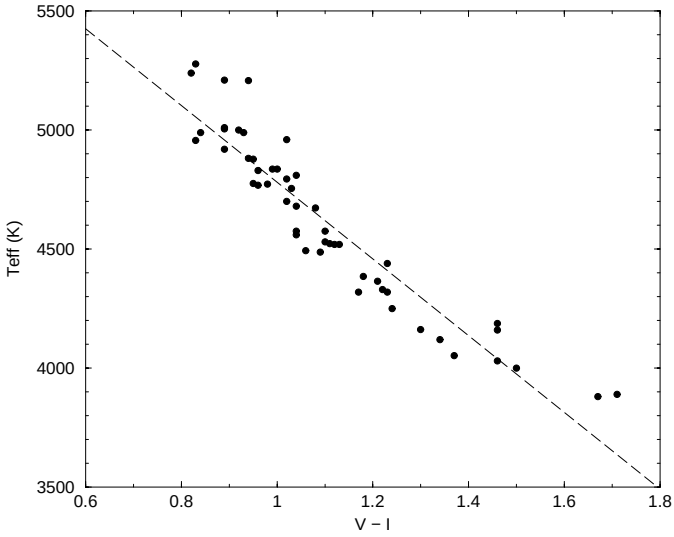

Fig. 2. Spectrally determined effective temperatures of sample giants versus $V-I$ color indices extracted from the Hipparcos catalogue. The dashed curve represents the calibration scale described by Eq. (2).

stars, 380 fell into one field of view of the Einstein Imaging Proportional Counter (IPC) and form the sample of Maggio et al.. The sample of Haisch et al. consists of 255 optically selected stars that have been observed by the IUE satellite. From these two samples, I extracted all luminosity class III stars of spectral type G and K and systematically rejected spectroscopic binaries known from the Bright Star Catalogue. This initial sample was complemented by an extraction of single G and K stars from a list of 144 giants with accurate rotational velocities measured by de Medeiros & Mayor (1995). Spectroscopic binaries were systematically excluded for two reasons. First, tidally enforced rotation in close binaries may induce a solar-type activity not present on a single star with identical mass at a similar evolution stage. Secondly, H-R diagram positions are not accurate for binaries.

Parallax values, V magnitude, $B-V$ and $V-I$ color indices have been obtained from the Hipparcos catalogue. From this sample, only stars with parallaxes greater that 4 milliarcsec were selected. Hence, the final sample consists of 88 apparently single G-K giants with reliable distance estimates. Spectral type and effective temperature of 54 stars (see Table 1) of this sample were found in the Catalogue of [Fe/H] determination from Cayrel de Strobel (1996). The spectrally determined effective temperatures of this subsample were combined with the Hipparcos $B-V$ and $V-I$ color indices to determine effective temperature calibration scales.

$$T_{\rm eff}(K) = 6577 - 1754(B-V) \quad (1)$$

$$T_{\rm eff}(K) = 6392 - 1611(V-I) \quad (2)$$

The temperature scales described by Eqs. (1) and (2) have been established using giants with near solar metallicity $-0.4 < [{\rm Fe/H}] < 0.4$. The two scales (see Figs. 1 and 2) provide consistent $T_{\rm eff}$ estimates for a homogeneous set of nearby single G-K giants. Hence, the effective temperature of the 34 remaining stars (see Table 2) were calculated from their Hipparcos color indices by averaging the $T_{\rm eff}$ estimates given by the two calibration scales. Since all of the giants are closer than 250 pc, no correction for reddening effect by interstellar absorption was applied. The standard deviation of the value estimated by this method with respect to the spectrally determined $T_{\rm eff}$ is 100 K.

The absolute magnitude of all giants were calculated from the V magnitude and parallaxes given in the Hipparcos catalogue. The stellar luminosities were derived from the absolute magnitudes using the bolometric correction vs effective temperature data of Flower (1996). Fig. 3 shows the positions of the sample giants in the H-R diagram. Fast rotating single active giants known as FK Comae type stars (see Table 1) are also represented in the H-R diagram of Fig. 3. These are FK Comae, YYMen (Collier Cameron 1982), HD 33798 (Fekel & Marschall, 1991), HD 199178 and HD 223460.

3. Evolutionary status of the sample stars

3.1. Comparison with evolutionary tracks

Positions of the sample stars in the H-R diagram were compared with evolutionary tracks inferred from grids of stellar models provided by Schaller et al. (1992). The logarithmic difference $[{\rm Fe/H}] = \log({\rm Fe/H}) - \log({\rm Fe/H})_{\odot}$ between the relative abundance of iron in the atmosphere of the sample giants and the relative abundance of iron in the solar atmosphere was retrieved from the Catalogue of [Fe/H] determination compiled by Cayrel de Strobel (1996). The histogram of the [Fe/H] distribution is given in Fig. 4. The average metallicity of the spectroscopic sample (see Table 1) is -0.13 dex. Still, 65 % of the sample giants with [Fe/H] determination have a metallicity relative to the Sun included between +0.2 dex and -0.2 dex. Hence, the H-R diagram positions of all sample stars were compared with

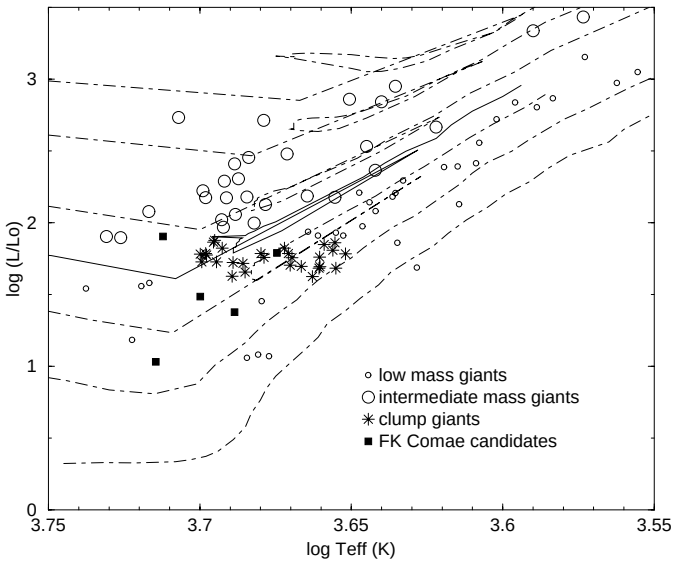

Fig. 3. H-R diagram of the sample giants compared with evolutionary tracks (Schaller et al. 1992) of 1 $M_\odot$, 1.5 $M_\odot$, 2 $M_\odot$, 2.5 $M_\odot$ (solid line), 3 $M_\odot$, 4 $M_\odot$ and 5 $M_\odot$ giants.

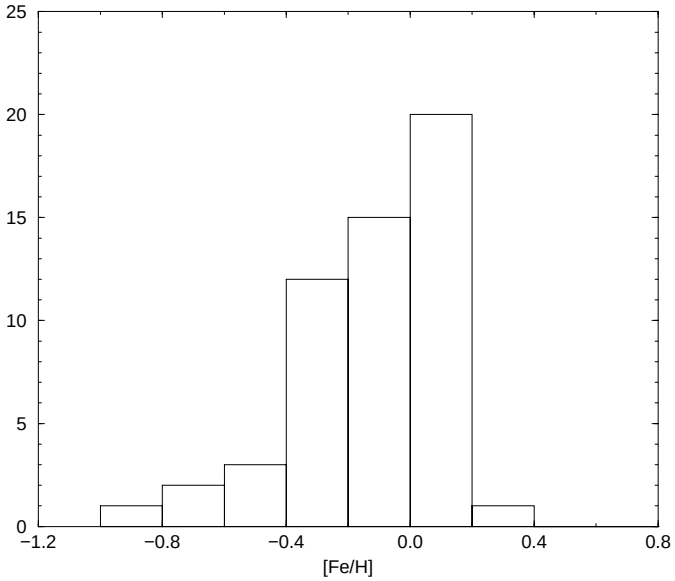

Fig. 4. Distribution of the logarithmic difference [Fe/H] between the relative abundance of iron in the atmosphere of sample giants and the relative abundance of iron in the solar atmosphere from Cayrel de Strobel (1996).

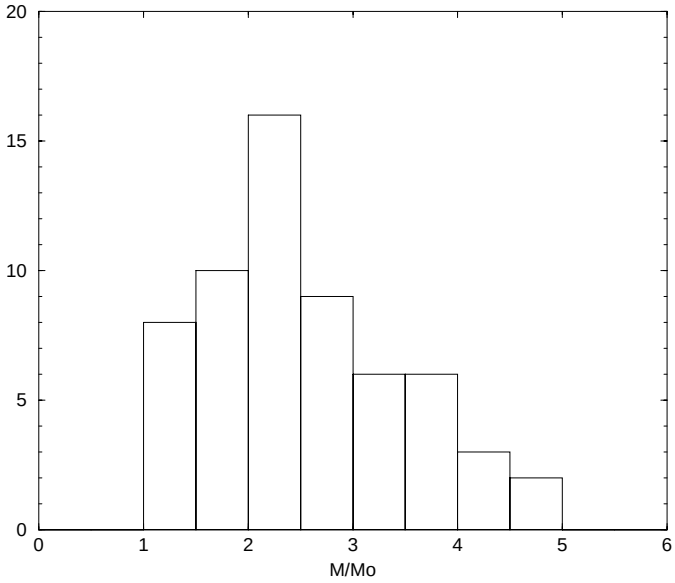

Fig. 5. Mass histogram of the sample giants located outside of the clump star region.

evolutionary model computed for a near solar metallicity (Z = 0.02). The models of Schaller et al. (1992) use opacities provided by Rogers & Iglesias (1992) and by Kurucz (1991) and their convection paramaters (i.e mixing length ratio and overshooting parameter) have been calibrated using the red giant branch of a wide range of clusters.

Stellar models predict a different evolution for low mass and intermediate-mass giants. Stars of masses below about 2.5 $M_\odot$ develop degenerate cores after central hydrogen exhaustion. They climb the red giant branch until a strong He-flash event lifts degeneracy and then settle on the core He-burning phase at an almost constant luminosity. This gives origin to the clump of red giant stars. Girardi et al. (1998) have used the Hipparcos database to determine the local distribution of clump giants in $M_{\rm V}$ versus $B-V$ and $M_{\rm I}$ versus $V-I$ diagrams. From the $T_{\rm eff}$ calibration scale given by Eqs. (1) and (2), the corresponding location of the local Hipparcos clump in the H-R diagram of Fig. 3 is given by $3.64 < log(T_{\rm eff}) < 3.71$ and $1.5 < log(L/L_\odot) < 1.9$ within a 3 σ dispersion of luminosity. Masses of the sample stars located outside of this clump star region were estimated from their position with respect to the theoretical evolutionary tracks assuming a first crossing of the H-R diagram. No correction for interstellar extinction was applied to their absolute magnitudes. The resulting underestimate of the stellar masses is less than 10 % for stars closer than 200 pc, i.e 95 % of the sample.

Mass estimates are listed in Table 2 together with rotational velocities (Medeiros & Mayor 1995, Gray 1989), X-ray luminosities (Maggio et al. 1990, Hünsch et al. 1998) and lithium abundances (Brown et al. 1989). Fig. 5 depicts the mass histogram of the sample stars located outside of the clumps star region. This includes 34 stars with $M < 2.5\ M_\odot$ and 26 stars with $2.5\ M_\odot \leq M < 5\ M_\odot$. These two subsamples will be called hereafter the low mass giants and the intermediate-mass giants respectively. The mass of the 28 clump giants have not been estimated since their evolutionary status is uncertain. Also the masses of the FK Comae candidates may be underestimated since the reference evolutionary tracks do not account for rotational effects. FK Comae masses are not included in the histogram shown in Fig. 5.

3.2. Lithium abundance

Li abundances measurements offer an alternative method to assess the evolutionary status of single giants. Results of Li abun-

dances measurements of 36 of the sample stars have been found in the Brown et al. (1989) catalogue. They are provided in Table 2. Among 13 measurements performed on the sample giants located in the clump star region, only 2 detections (HD 6903 and HD 163993) are reported, thus indicating that most of these stars are in an advanced stage of evolution probably in their helium core burning phase. Indeed, as giants ascend the RGB, the inward expansion of their convective envelope transports Li and other light elements from the surface to the interior thus reducing their surface abundance by dilution. Once the giants have reached the helium core burning stage, their fully formed convective envelope is expected to have completely diluted the surface lithium remaining at the end of the main sequence lifetime. Hence, the two clump giants of the sample on which surface Li has been detected are most likely in an earlier phase of evolution. It is worth noting that they both are X-ray emitters.

Lithium has been detected on 10 other sample stars, 7 of which have masses $\geq 2.5\ M_{\odot}$. Upper limits have been found for an additional 14 stars of which 10 have masses $< 2.5\ M_{\odot}$. Li abundance seems therefore to be mainly found on intermediate-mass giants and less often detected on low mass ($M < 2.5\ M_{\odot}$) giants. The average masses of giants for which $\log(\epsilon(\mathrm{Li})) \geq 0.5$ and $\log(\epsilon(\mathrm{Li})) \leq 0$ are respectively $3.3 \stackrel{+}{-} 0.9\ M_{\odot}$ and $1.8 \stackrel{+}{-} 0.4\ M_{\odot}$. Fig. 6 shows the Li abundance vs effective temperature of the sample stars. The largest Li abundance is found for three $\geq 2.5\ M_{\odot}$ Hertzsprung gap G giants. Their $\log(\epsilon(\mathrm{Li})) = 1.3$ value is consistent with Iben's (1967) models for a $3\ M_{\odot}$ assuming that lithium is present at a constant abundance $\log(\epsilon(\mathrm{Li})) = 3.1$ in a thin layer of $1.3\ \%$ by mass at the surface of the main sequence progenitor. This indicates that cool giants with Li have evolved from early A and late B main-sequence progenitors. Their Li abundance at the bottom of the red giant branch suggests that their main sequence progenitors retained the primordial lithium over the shallow layer predicted by the standard Iben models. These stars have not depleted their Li while on the main sequence and had not enough time for sufficient convective mixing during their rapid evolution across the Hertzsprung gap. At the same stage of evolution, i.e near the bottom of the RGB, Li seems to be already depleted in the outer-most convective layers of most of the low mass stars of the sample which have early F and late A progenitors. This is consistent with surface Li abundance calculations performed by Richer & Michaud (1993) as a function of temperature along the evolutionary track of 1.2 to 2.2 $M_{\odot}$ stars. After a first Li enrichment at the surface of 2 $M_{\odot}$ stars at the early F giant stage, their calculation predicts a Li depletion up to a factor of 10 or larger for temperatures between 6600 and 6500 K when the convection zone increases further in depth.

Li abundance measurements on sample giants with $T_{\mathrm{eff}} < 4800$ suggest a decline of $\log(\epsilon(\mathrm{Li}))$ with decreasing effective temperature as illustrated in Fig. 6. Such a behavior is expected from the classical first dredge-up theory. Indeed, at the end of the main sequence lifetime, Li can exist only in the top 0.5% to 3%, approximately, by mass of a star and the red giant envelope itself is too cool to cause further destruction of lithium. However, as the star evolves up the RGB, the convective envelope expands

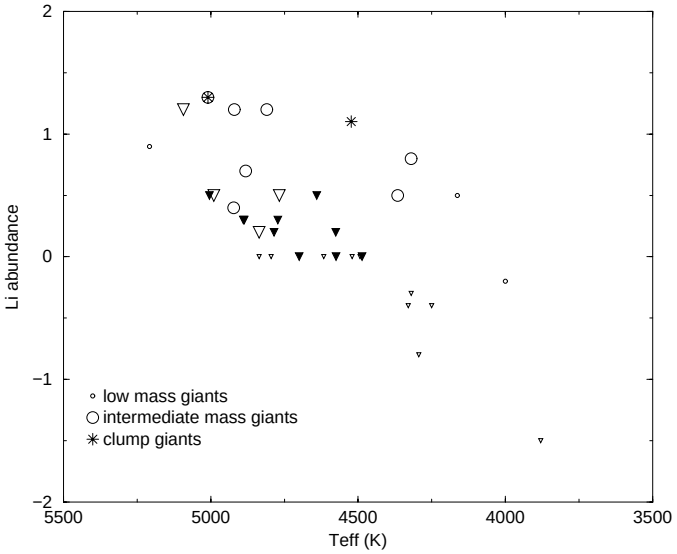

Fig. 6. Lithium abundances of the sample giants. Upper limits of Li abundances are indicated by small triangles, large triangles and filled triangles for low mass, intermediate- mass and clump giants respectively. For comparison, the cosmic Li abundance is $\log(\epsilon(\mathrm{Li})) = 3.2$ and the present solar Li abundance is $\log(\epsilon(\mathrm{Li})) = 1.0$ (Aller & Ross 1976) on a scale where the logarithmic hydrogen abundance is 12.

inwards and mixes an increasing fraction of the stellar mass thus explaining why surface Li is more depleted on K giants with cooler effective temperatures. The range of Li abundance shown at a given temperature in Fig. 6 is partially due to the range of masses, with no Li detection on the lower mass stars. The lower envelope drawn in Fig. 6 by low mass stars results from the fact that the upper limit abundance value to which Li can be detected decreases with temperature (Brown et al. 1989). Hence, the Li distribution on the sample giants is consistent with their evolutionary status as inferred from comparison with evolutionary tracks. It suggests that $\geq 2.5\ M_{\odot}$ stars could retain primordial lithium on their surface during their evolution till the bottom of the RGB while Li is depleted earlier in the evolution of lower mass stars maybe as they move off the main sequence.

4. Observational data survey

4.1. Rotational velocities

Accurate $v \sin i$ measurements obtained with CORAVEL by de Medeiros & Major (1995) or by Gray (1989) have been found for 59 stars of the sample. They are listed in Table 2. The CORAVEL $v \sin i$ measurements, which are precise to about $1\ \mathrm{km\,s^{-1}}$, are plotted in Fig. 7 as a function of T_{eff} for different mass ranges. Low mass stars ($M < 2.5 M_{\odot}$) and clump giants have low rotational velocities ($v \sin i < 10\ \mathrm{km\,s^{-1}}$). FK Comae candidates, on the contrary, have the highest $v \sin i$ ($> 30\ \mathrm{km\,s^{-1}}$). The rotation of intermediate-mass giants evolves in a remarkable way. Indeed, their projected equatorial velocities decrease with effective temperature till T_{eff} = 4700 K where a minimum $v \sin i$ value of 1 or $2\ \mathrm{km\,s^{-1}}$ is reached.

Simon & Drake (1989) noticed a smooth decline of $v \sin i$ for giants later than G0 III. They suggest together with Gray (1989) that magneto-hydrodynamic braking due to stellar winds decreases the rotational velocities of giants when they evolve to lower effective temperatures. Also, Schrijver & Pols (1993) indicated that the loss of angular momentum through magnetic braking is substantial in the evolution of giants between the onset of convection and just beyond the upturn on the giant branch. On the other hand, Rutten and Pylyser (1988) argued that during the entire evolution of a 3 $M_{\odot}$ star the timescale for magnetic braking is larger than the evolutionary time scale. Endal & Sofia (1979) and Gray & Endal (1982) pointed out that the expansion of the stars on the red giant branch together with the rearrangement of angular momentum due to the increasing depth of the convection zones may well explain the decrease of $v \sin i$ for cool giants. One extreme case of rotation rate evolution is the situation where no radial exchange of angular momentum occurs in the expansion of the giants envelope. The rotation velocity can then be estimated as a function of effective temperature according to Eq. (3) from the change in the total radius.

$$v(T_{\rm eff}) = v_{\rm ZAMS}.R_{\rm ZAMS}/R(T_{\rm eff}) \quad (3)$$

where $R_{\rm ZAMS}$ and $v_{\rm ZAMS}$ are the radius and the rotational velocity of the star on the zero-age main sequence (ZAMS). During their evolution towards the bottom of the ascending giant branch from $T_{\rm eff}$ = 5500 K to $T_{\rm eff}$ = 4800 K, the radii of intermediate-mass giants increase by at most a factor of 2 while Fig. 7 indicates that rotational velocities decrease by at least one order of magnitude. Hence, Fig. 7 shows that the rotational velocities of intermediate-mass giants depart from specific angular momentum conservation of the surface layers as the stars evolve towards the bottom of the red giant branch. Under the assumption of total angular momentum conservation, Endal and Sofia (1979) calculated that for stars with deep convective envelopes the velocities resulting from complete radial exchange of angular momentum are smaller than estimated by Eq. (3) by a factor of about three. This is a consequence of the lower degree of inner mass density of the convective envelope of red giants as compared with the radiative envelope of their main sequence progenitors. The observed evolution of $v \sin i$ vs $T_{\rm eff}$ for intermediate-mass giants confirms the conclusion that the decrease in rotation velocities for giants with $T_{\rm eff} > 4700$ K is not only due to the expansion of the stars along the giant branch. If the effect of magnetic braking is small in the absence of strong stellar winds, important angular momentum redistribution is needed within the expanding convective envelope to explain the rapid evolution of the rotational velocity of giants as they approach the bottom of the red giant branch.

4.2. X-ray luminosities

Einstein X-ray fluxes from Maggio et al. (1990) were found for 10 giants of the sample. Count rates of 12 other sample stars were extracted from ROSAT source catalogue (Hünsch et al. 1999). These count rates were converted into X-ray fluxes using an energy conversion factor of 4.10^{-12} ergs cts^{-1} cm^{-2} (Hünsch et al. 1996). X-ray fluxes of 4 additional giants were obtained from the ROSAT all-sky survey catalogue of optically bright late-type giants and supergiants (Hünsch et al. 1998). I calculated the X-ray luminosities ($L_{\rm X}$) of all X-ray detected stars from the Hipparcos parallaxes. X-ray luminosities of a few giants based on the accurate Hipparcos distances have been previously reported by Micela et al. (1997). The results are presented in Fig. 8 as a function of $T_{\rm eff}$ for the different mass ranges. In case of multiple observations, the highest and lowest measured luminosities are plotted and the extrapolated X-ray luminosity range of the star is represented by a vertical bar. Upper limits of X-ray luminosities measured with the Einstein observatory (Maggio et al. 1990) are indicated by triangles for the different subsamples. The X-ray luminosities of the active FK Comae stars are marked with black squares. One of the giants listed in Table 2 (HD 145000) was not included in Fig. 8 since its *Einstein* X-ray detection most likely originates from the coronae of its hotter G8 III visual companion (Maggio, private communication).

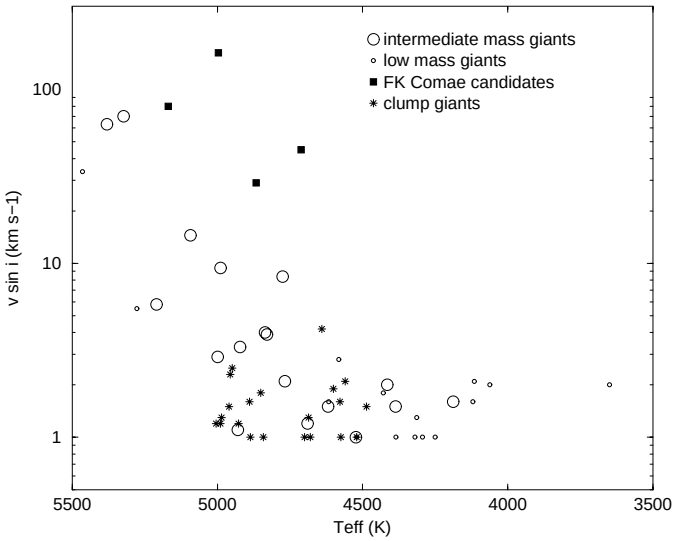

Fig. 7. Rotational velocities of the sample giants.

Fig. 8 shows a transition from high X-ray luminosities to luminosities lower than 10^{29} erg s^{-1} at an effective temperature of about 4700 K. This corroborates the well known existence of an X-ray dividing line (XDL) at spectral type K1 (Ayres et al. 1981). At $T_{\rm eff} > 4800$ K, the X-ray luminosities of giants often exceed 10^{29} erg s^{-1}. Thirteen giants have $L_{\rm X} \geq 10^{30}$ erg s^{-1}. At $T_{\rm eff} < 4700$ K, *Einstein* measurements (Maggio et al. 1990) of the sample stars only provide upper limits often smaller than 10^{29} erg s^{-1}. On this right side of the XDL, only four ROSAT detections are reported among the sample stars (Schröder et al. 1998), three of which have an X-ray luminosity close to 10^{27} erg s^{-1}. No sign of multiplicity is reported on any of these stars, including the most X-ray luminous one, HD 93813. Also, Hünsch et al. (1998) reported X-ray emission on the right side of the XDL from a few apparently single M type giants.

The most X-ray luminous giants of the sample have masses of about 3 $M_{\odot}$. On the left side of the XDL, X-ray emission has been detected mainly on $M \geq 2.5\, M_{\odot}$ giants. Hence, Fig. 8

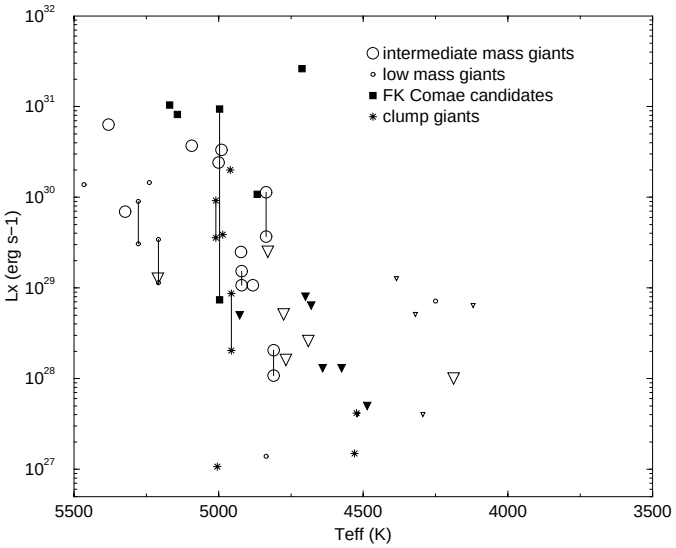

Fig. 8. X-ray luminosities of the sample giants. Upper limits of X-ray luminosities (Maggio et al. 1990) are indicated by small triangles, large triangles and filled triangles for low-mass, intermediate- mass and clump giants respectively.

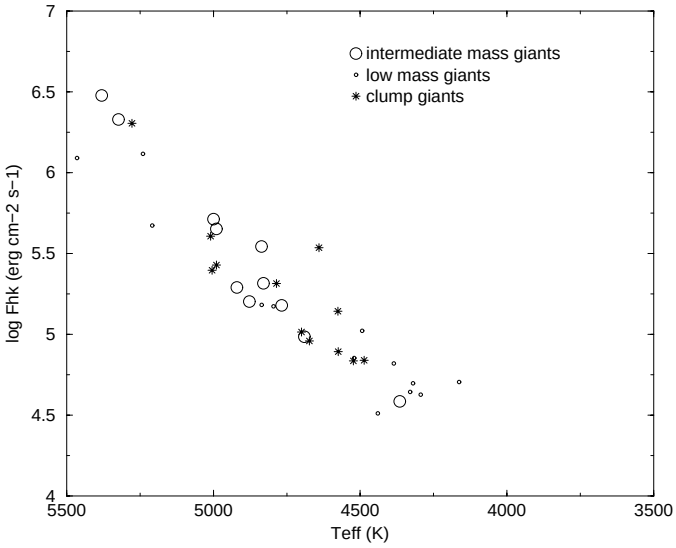

Fig. 9. Logarithm of the Ca II H and K surface emission fluxes of the sample giants.

confirms the existence of an X-ray dividing line around spectral type K1, but for intermediate-mass stars only. A few detections of lower mass giants ($M < 2.5\,M_{\odot}$) are reported on the left side of the XDL but at lower X-ray luminosity levels or at effective temperature higher than 5200 K. X-ray activity on low mass giants seems to decay earlier in their evolution.

4.3. Ca II emission fluxes

Emission in the cores of the Ca II H and K lines is an other important indicator of stellar activity. It is produced by a temperature rise above the photosphere that indicates that the atmosphere is not in radiative equilibrium. By analogy with the Sun, the source of this excess heating is thought to be produced by magnetic processes on cool dwarf stars. For evolved stars, however, different scenarios have been proposed involving hydrodynamic phenomena and acoustic processes (Cuntz et al. 1994). Calibrated Ca II H and K fluxes of 33 sample giants were found in the extensive tabulation of measured values of the Ca II H and K emission flux compiled by Young et al. (1989). These authors used the recipe given by Middelkoop (1982) to convert the S-index defined by Vaughan et al. (1978) into a flux emitted at the stellar surface. The logarithm of the Ca II emission fluxes of the 33 sample giants is plotted in Fig. 9 as a function of effective temperature. Intermediate-mass giants have statistically higher effective temperatures and Ca II emission fluxes than low mass giants. However, Fig. 9 indicates that low mass giants, intermediate-mass giants and clump giants follow a similar Ca II flux dependence with effective temperature. Stellar effective temperature is a major parameter in determining the level of chromospheric Ca II radiative losses among $< 5M_{\odot}$ G and K giants. A relationship between chromospheric surface activity and effective temperature was established by Pasquini & Brocato (1992) on a sample of cool giants and supergiants. This relationship also involves stellar mass to account for the higher level of chromospheric activity measured on massive (5–10 $M_{\odot}$) evolved stars (Pasquini et al. 1990).

Fig. 9 shows that the Ca II emission of the sample giants decreases smoothly with decreasing effective temperature. No evidence is found for a sharp decline in the surface flux of Ca II at an effective temperature of 4700 K. A smoothly decreasing Ca II flux with increasing V-R color index was recently reported by Dupree et al. (1999) on a sample of 15 red giants located in the open cluster M67. These authors noted that the same smooth color dependence of net Ca II flux was present on a sample of field giants studied by Pasquini et al. (1990). These results contrast with the sharp transition from high to low X-ray luminosity observed at an effective temperature of 4700 K on the sample giants. The smooth decrease of Ca II emission also differs from the substantial decline in Si IV emission (Ayres et al. 1997) and C IV emission (Böhm-Vitense 1992) measured on single giants on the right side of the XDL compared with their counter part at the red edge of the Hertzsprung gap. To explain these different behaviours, Dupree et al. (1999) suggested that chromospheric Ca II emission on the red giant branch arises from a combination of magnetic and nonmagnetic heating processes, with the magnetic component decreasing in importance as the star evolves up the red giant branch. Coronal X-ray emission, on the contrary, would be magnetically dominated.

5. Discussion

5.1. Relationship between X-ray luminosity and rotation

The survey of observational data indicates a minimum in rotational velocity below 4800 K and a sharp decrease of X-ray emission at this same effective temperature for intermediate-mass giants. These $v \sin i$ and X-ray measurements were however performed on two different samples of stars. Their effec-

tive temperature distributions between 5600 K and 3600 K were compared with that of the $M \geq 2.5\ M_{\odot}$ population of the initial sample using Pearson's χ^2 test. χ^2 values of respectively 1.69 and 2.42 were obtained with 5 degrees of freedom. This indicates that the two subsamples can be considered as representative of the same population of intermediate-mass giants with a confidence level of 67% to 80%. Hence, an important result of this study is that the sharp decay of X-ray emission at spectral type K1 likely occurs in the coronae of intermediate-mass giants as their surface rotational velocities reach a minimum.

This result suggests that the intensity of coronal X-ray emission among intermediate-mass G and K giants should be correlated with the evolution of their rotational velocities as they approach the bottom of the red giant branch. However, no tight correlation between X-ray emission and rotational velocities close to the XDL has been reported before (Böhm-Vitense 1992). Tentative explanations for this lack of relationship argued that measured X-ray fluxes often refer to binaries which have higher X-ray luminosities than single giants. Fig. 10 shows the X-ray luminosity as a function of projected equatorial velocity for those of the sample single giants on which both measurements are available. Fig. 10 illustrates the absence of a tight relationship between X-ray luminosities and projected equatorial velocities close to the X-ray dividing line. Indeed, some giants with $v \sin i < 10\,\mathrm{km\,s^{-1}}$ exhibit X-ray luminosities higher than 10^{29} erg s^{-1}. Apparently these stars do not follow the $L_{\mathrm{X}} = 10^{27}\ (v \sin i)^2$ dependence discovered by Pallavicini et al. (1981) on a sample of late type stars that included binaries and dwarfs but only few single G-K giants. Apart from the FK Comae candidates, most of the sample giants present an excess of X-ray luminosity compared with this general trend by more than one order of magnitude which cannot be accounted for by the variability of their X-ray emission. A reason could be that verification of the $L_{\mathrm{X}} = 10^{27}\ (v \sin i)^2$ dependance for slowly rotating G or K giants is biased by upper detection limits which for the ROSAT all sky survey typically equals 1.5 10^{28} erg s^{-1} at 35 pc (Schröder et al. 1998). If the $L_{\mathrm{X}} = 10^{27}\ (v \sin i)^2$ relationship applies to giants close to the XDL, X-ray luminous giants with low $v \sin i$ ought to be stars seen pole-on for which equatorial velocities exceeds $10\,\mathrm{km\,s^{-1}}$. Such an explanation is unlikely since the $v \sin i$ distribution shown on Fig. 7 indicates that the occurence probability of equatorial velocities greater than $10\,\mathrm{km\,s^{-1}}$ is low close to the XDL. Hence, X-ray luminosities and rotational velocities are not correlated on giants evolving near the bottom of the red giant branch. A parameter other than $v \sin i$ must play a crucial role in determining the X-ray emission level of stars located on the left side of the XDL.

5.2. Evolution of X-ray activity along the giant branch

Masses of the sample giants have been estimated assuming a first crossing of the H-R diagram. Within the limit of this hypothesis, the T_{eff} dependence of X-ray emission, rotation velocities and lithium abundances among $\geq$2.5 $M_{\odot}$ G-K giants can be explained in term of stellar evolution as follows. G-K giants with $M \geq 2.5\ M_{\odot}$ have A and late B type progenitors on the main sequence which have no outer convection zones and which are usually rapid rotators. They lose little angular momentum during their dwarf phase. Only as they evolve through the Hertzsprung gap, in the shell hydrogen burning stage, do they develop outer convection zones. The combination of rapid rotation with convection induces a large degree of magnetic activity on the basis of the standard dynamo theory. In the Sun, both chromospheric Ca II and coronal X-ray emission are known to be well correlated with surface magnetic fields. As a result $\geq 2.5\ M_{\odot}$ giants crossing the Hertzsprung gap are strong Ca II and X-ray emitters. Magnetic fields were indeed directly measured on two G giants of the sample (HD 28305 and HD 163993) by means of the Babcock-technique (Hubrig et al. 1994).

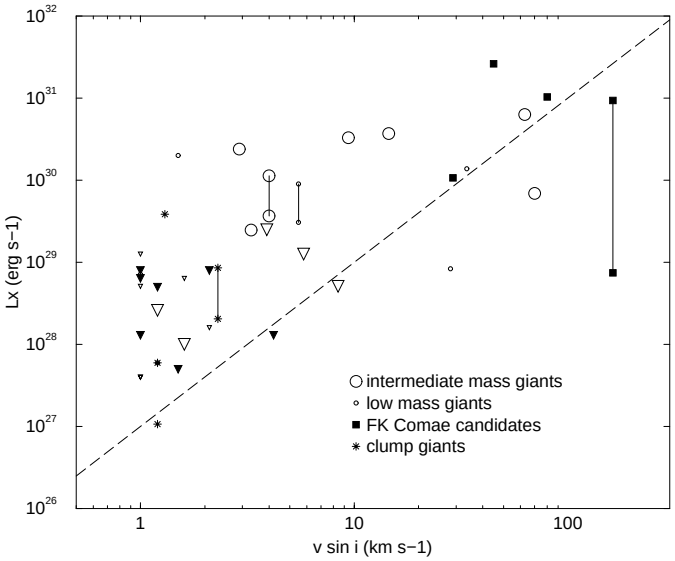

Fig. 10. X-ray luminosities of the sample giants as a function of rotational velocities. Upper limits of X-ray luminosities are indicated by small triangles, large triangles and filled triangles for low-mass, intermediate- mass and clump giants respectively. For comparison, the Lx=$10^{27}(v \sin i)^2$ relationship (Pallavicini et al. 1981) is indicated by a dashed line.

Rapidly rotating, chromospherically active stars classified as FK Comae stars could be in that short stage of evolution. Envelope expansion might have been less efficient in reducing their rotation rates if they have rapidly evolved from fast rotating A and B progenitors. Rapidly rotating stars behave as less massive non rotating stellar models which masses along the non rotating ZAMS are highly concentrated towards the center, as evidenced by their large central densities and pressures. Core contraction at the red giant stage decreases the moment of inertia, which increases the rotation rate and leads to central condensation, etc... Thus a positive feedback loop exists which operates preferentially in stars with rapid rotation rates such as FK Comae giants. Rotational velocities on the giant branch is therefore significantly higher for these stars than given by Eq. (3) till the envelope expansion decreases the rotation rate sufficiently that the positive feedback loop become unimportant. This mechanism suggested by Endal and Sofia (1979) could explain the high rotation velocities of FK Comae candidates (see Table 2)

and of some G giants (e.g HD 6903 and HD 111812) at effective temperature around 5000 K (see Fig. 7). The rotational velocities of these stars on the main sequence may have been close to brake up. Also, their positions in the H-R diagram indicates that their envelope have not expanded enough to sufficiently decrease the initial rotation rate. A positive feedback loop due to core contraction may still be important on these stars. FK Comae type stars could then have evolved from those of the early A or late B single stars which have the highest rotational velocities. The positive feedback loop suggested by Endal and Sofia is an alternative hypothesis to the W UMa-system merger model proposed by Rucinski (1990) to explain the high rotation rates of FK Comae giants.

As indicated by Danziger and Faber (1972), the initial expansion of the stellar envelope which occurs as giants cross the Hertzsprung gap likely induces differential rotation. This maintains a high activity level in spite of the decreasing rotational velocities. As the stars reach the base of the ascending red giant branch, deep mixing occurs due to the increasing depth of the convection zone expected theoretically and indicated by the decrease of Li surface abundance (see Fig. 6). This results in a radial exchange of angular momentum which could induce most of the rotational braking. If so, a large viscosity induced by turbulent convection can be expected which would tend to restore rigid rotation. The absence of a tight correlation between X-ray luminosity and surface rotational velocities close to the XDL perhaps reflects the importance of differential rotation in determining the intensity of coronal emission among giants. Not only the rotational braking per se but also the restoration of rigid rotation through complete exchange of angular momentum at the bottom of the RGB could prevent the maintenance of strong magnetic fields through the α-Ω dynamo mechanism. This speculative scenario could explain both the absence of relationship between X-ray luminosity and rotation rate and the observed location of the XDL at a position in the H-R diagram where the projected equatorial velocities of intermediate-mass giants are a minimum. Gilliland (1985) indicated that the spin-down process has the effect of increasing the Rossby number, and hence leads to a decrease in classical, helicity related, dynamo-driven activity. Rosner et al. (1995) remarked that this suppression of a large-scale dynamo need not imply the suppression of magnetic field production at small scales, driven by the turbulent motions in the convection zones of the giants. They suggest rather that a large scale organized surface magnetic flux emergence normally associated with stellar activity disappears, and is replaced by small-scale magnetic flux emergence arising from a weak seed field placed in a turbulent convection zone. The atmosphere of giants on the red side of the XDL would then become largely opened on large spatial scales. Closed structures could remain if their spatial scale falls below the atmosphere's pressure scale height (Antiochos et al. 1986). These remaining X-ray emitting loops would become cool and the open-field regions may not be able to retain a hot coronal plasma due to the decreasing gravity of giants as they evolved up the RGB. The coronal emission of giants would then be shifted towards longer wavelength thus explaining the sharp decrease of coronal X-ray emission at spectral type K1.

6. Summary

The present study uses recently available stellar parallaxes provided by the Hipparcos star catalogue (ESA 1997) to determine the position of field giants into a theoretical H-R diagram and to estimate their masses. The evolutionary status of the sample giants is consistent with their surface Li distribution. It suggests that $\geq 2.5\ M_{\odot}$ stars could retain primordial lithium on their surface during their evolution till the bottom of the RGB while Li is depleted earlier in the evolution of lower mass stars. Previously published X-ray luminosities and rotational velocities of single giants are examined as a function of effective temperature and newly determined masses. The results confirm the existence of a sharp decrease of X-ray emission at an effective temperature of 4800 K but only for intermediate-mass giants ($2.5\ M_{\odot} \leq M < 5\ M_{\odot}$). The study shows that this sharp decay of X-ray emission occurs in the coronae of intermediate-mass giants as their surface rotational velocities reach a minimum value of 1 to 2 km s^{-1}. No tight relationship is found between the X-ray luminosities and the rotational velocities of the sample stars. I suggest that this results reflects the importance of differential rotation in determining the level of coronal activity among giants. Not only the rotational braking per se but also the restoration of rigid rotation could prevent the maintenance of strong magnetic fields at the bottom of the red giant branch, thus explaining the sharp decrease of coronal X-ray emission at spectral type K1.

This conclusion supports the hypothesis that the coronal structure of intermediate-mass giants could change from large scale magnetic structures to compact coronal loops as the stars evolve near the bottom of the red giant branch. X-ray spectroscopy is the appropriate tool to survey the magnetic structure of the coronae of late-type stars and to test this evolution scenario. In particular, the ESA high throughput X-ray spectroscopic mission (XMM) will resolve individual lines from different ionization stages of various abundant elements which provides a direct diagnostics of a variety of coronal plasma parameters. The combination of emission measures and electron densities measurements can be used to predict the effective volume of emitting plasma at different temperatures and to identify compact structures similar to magnetically confined coronal loops. By comparing the coronal structure of giants having different evolutionary status, new X-ray observatories such as XMM and Chandra will bring further constraints on the relationship between rotation and the dynamo generation of stellar magnetic fields.

Acknowledgements. I thank Drs A. Maggio and F. Favata and the referee, Dr. J. Linsky, for providing helpful comments on earlier versions of the manuscript.

References

Aller L.H., Ross J.E., 1976, Sci 191, 1223
Antiochos S.K., Haisch B.M., Stern R.A., 1986, ApJ 307, L55
Ayres T.R., Linsky J.L., Vaiana G.S., et al., 1981, ApJ 250, 293
Ayres T.R., Brown A., Harper G.M., et al., 1997, ApJ 491, 876
Böhm-Vitense E., 1992, AJ 103, 608
Brown J.A., Sneden C., Lambert D.L., et al., 1989, ApJS 71, 293
Cayrel de Strobel G., Soubiran C., Friel E.D., et al., 1996, A&AS 124, 299
Collier Cameron A., 1982, MNRAS 200, 489
Cuntz M., Ranmacher W., Ulmschneider P., 1994, ApJ 432, 690
Danziger I.J., Faber S.M., 1972, A&A 18, 428
Dupree A.K., Whitney B.A., Pasquini L., 1999, ApJ 520, 751
Endal A.S., Sofia S., 1979, ApJ 232, 531
ESA, 1997, The Hipparcos Catalogue, ESA SP-1200
Fekel F.C., Marschall L.A., 1991, AJ 102, 1439
Flower P.J., 1996, ApJ 469, 335
Gilliland R.L., 1985, ApJ 299, 286
Girardi L., Groenewegen M.A.T., Weiss A., Salaris M., 1998, MNRAS 301, 149
Gondoin P., Mangeney A., Praderie F., 1987, A&A 174, 187
Gray D.F., 1989, ApJ 347, 1021
Gray D.F., Endal A.S., 1982, ApJ 254, 162
Haisch B.M., Bookbinder J.A., Maggio A., Vaiana G.S., Bennet J.O., 1990, ApJ 361, 570
Hoffleit D., Saladyga M., Wlasuk P., 1984, A Supplement to the Bright Star Catalog. Yale University Press, New Haven
Hubrig S., Plachinda S.I., Hünsch M., et al.,1994, A&A 291, 890
Hünsch M., Schmitt J.H.M.M., Sterzik M.F., Voges W., 1999, A&AS 135, 319
Hünsch M., Schmitt J.H.M.M., Schröder K.P., et al., 1996, A&A 310, 801
Hünsch M., Schmitt J.H.M.M., Voges W., 1998, A&AS 127, 251
Hünsch M., Schmitt J.H.M.M., Schröder K.P., et al., 1998, A&A 330, 225
Iben I. Jr., 1967, ApJ 147, 624
Kurucz R.L., 1991, In: Stellar Atmospheres: Beyond Classical Models. NATO ASI Series C, Vol. 341
Maggio A., Vaiana G.S., Haisch B.M., et al., 1990, ApJ 348, 253
de Medeiros J.R., Mayor M., 1995, A&A 302, 745
Micela G., Favata F., Sciortino S., 1997, A&A 326, 221
Middelkoop F., 1982, A&A 113, 1
Pallavicini R., Golub L., Rosner R., et al., 1981, ApJ 248, 279
Pasquini L., Brocato E., Pallavicini R., 1990, A&A 234, 277
Pasquini L., Brocato E., 1992, A&A 266, 340
Richer J., Michaud G., 1993, ApJ 416, 312
Rogers F.J., Iglesias C.A., 1992, ApJS 79, 507
Rosner R., Musielak Z.E., Cattaneo F., Moore R.L., Suess S.T., 1995, ApJ 442, L25
Rucinski S.M., 1990, PASP 102, 306
Rutten R.G.M., Pylyser E., 1988, A&A 191, 227
Schaller G., Schaerer D., Meynet G., Maeder A., 1992, A&AS 96, 269
Schrijver C.J., Pols O.R., 1993, A&A 278, 51
Schröder K.P., Hünsch M., Schmitt J.H.M.M., 1998, A&A 335, 591
Simon T., Drake S.A., 1989, ApJ 346, 30
Vaughan A.H., Preston G.W., Wilson O.C., 1978, PASP 90, 267
Young A., Ajir F., Thurman G., 1989, PASP 101, 1017